Isopycnal Dispersion in NATRE

KURT POLZIN

Woods Hole Oceanographic Institution, Woods Hole, Massachusetts

RAFFAELE FERRARI

Massachusetts Institute of Technology, Cambridge, Massachusetts

(Manuscript received 22 May 2002, in final form 22 May 2003)

ABSTRACT

Finescale velocity and density fluctuations consist of both internal waves and vorticity-containing perturbations (vortical modes). A recent decomposition of observations obtained as part of the North Atlantic Tracer Release Experiment (NATRE) permits one to investigate isopycnal stirring associated with vortical modes. This stirring is treated here as a relative dispersion problem in the context of 2D turbulence. Isopycnal diffusivities attain values on the order of 1 $m^2\ s^{-1}$ after an initial transient of 5–10 days. After 2 weeks, a patch of tracer with initial radius of 25 m is predicted to have evolved into a convoluted web having an rms radius of 2–4 km. These estimates agree with observations of the evolution of an anthropogenic tracer in NATRE.

1. Introduction

Dispersion of tracers in the ocean interior, away from boundaries, is dominated by adiabatic motions along density surfaces (isopycnal dispersion) rather than by diabatic three-dimensional turbulence. Adiabatic motions include a variety of different processes from mesoscale eddies, to submesoscale vorticity perturbations, and internal waves. All contribute to dispersion, but with different efficiencies. The goal of this paper is to study the dispersion of a tracer patch released in the midocean thermocline and to determine which motions control the isopycnal spreading of the tracer patch over the first few weeks after release.

Dispersion of a tracer patch in a turbulent flow field is achieved through persistent straining and the ensuing filamentation of the patch. The rate of dispersion associated with turbulent eddies of any given scale depends upon their size relative to the size of the patch. The advection of a tracer patch by an eddy having a scale much larger than the area of the patch results in a quasi-coherent translation (meandering) rather than dispersion. Eddies of size similar to the patch area act as a coherent rate of strain and efficiently deform the initial patch through filamentation, thus accelerating the tracer dispersion. Eddies much smaller than the patch size act incoherently and spread the patch at a much slower diffusive rate. Whether big eddies or small eddies dominate the dispersion of a tracer patch of a certain size depends upon their amplitude relative to eddies of size comparable to the patch area.

In contrast to fully developed turbulence, the internal wave field is inefficient at dispersing tracers. A single internal wave is nondispersive in the sense that tracer particles wind up at their original positions after a wave period, and thus experience no net displacement. Dispersion by internal waves appears only as a second-order Stokes drift effect, due to nonresonant wave–wave interactions (Sanderson and Okubo 1988; Ferrari 2003, unpublished manuscript), and through the coupling of internal wave shear to vertical mixing (shear dispersion; Young et al. 1982).

In this paper we focus on dispersion due to motions with horizontal scales between 10 m and 10 km. In this range of scales, the oceanic velocity field is dominated by internal waves. However, Polzin et al. (2003) have recently shown that internal waves coexist with quasi-permanent potential-vorticity-carrying perturbations referred to as vortical modes. If vortical modes can be characterized as a turbulent process, they can dominate finescale dispersion despite having much smaller velocities than internal waves.

An anthropogenic tracer (SF_6) was released on an isopycnal as part of the North Atlantic Tracer Release Experiment (NATRE; Ledwell et al. 1998). The tracer was clearly teased into filaments by the mesoscale eddy field. Given observations of the length and width of the filaments, Ledwell et al. (1998) infer the presence of a finescale stirring agent with an isopycnal diffusivity of

Corresponding author address: Dr. Kurt Polzin, Woods Hole Oceanographic Institution, MS #21, Woods Hole, MA 02543-1541. E-mail: kpolzin@whoi.edu

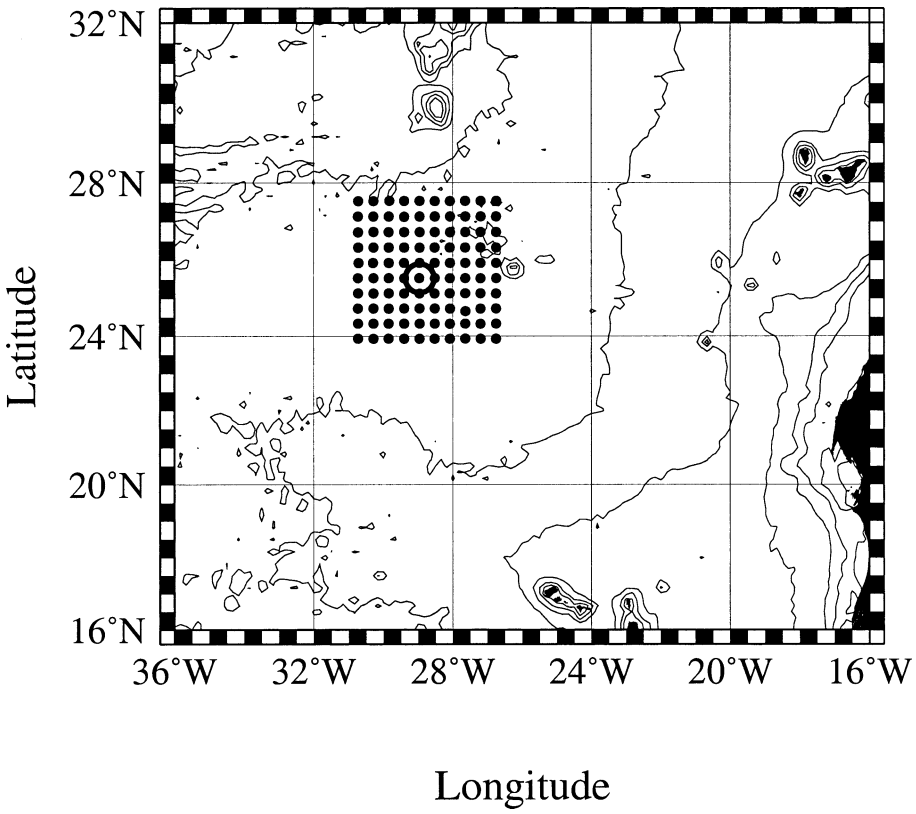

FIG. 1. Location of NATRE. HRP deployment positions of a large-grid survey are indicated as dots. The open circle at (25.5°N, 29°W) denotes the position of a current-meter mooring deployed as part of the subduction experiment. Finer-scale HRP surveys and the tracer deployment were just to the northeast of the mooring.

1–2 $m^2 s^{-1}$. They consider this too large to be associated with internal waves. Here we attempt to quantify the stirring properties of subinertial vortical modes in NATRE. We do so by drawing upon a large body of work (e.g., Rhines 1979; Provenzale 1999) concerning 2D and quasigeostrophic turbulence and a recent documentation of the vortical field using high-resolution profiler (HRP) data from NATRE (Polzin et al. 2003).

The decomposition of the finescale field is described in section 2. The dispersive properties of this field are investigated in section 3. Results from the tracer release experiment for the first six months are discussed in detail in section 4. Our main result is that stirring by finescale vortical modes provides a framework to interpret the dispersion of tracer spots released in the ocean interior. Discussion and summaries conclude the paper.

2. The vortical mode spectrum

NATRE took place in the southeastern portion of the subtropical gyre (Fig. 1). The subinertial kinetic energy is relatively low, $(u^2 + v^2)^{1/2} < 3$ cm s^{-1}, and the θ–S relation at the level of the tracer release, $\sigma_\theta = 26.75$ kg m^{-3} or about 313 dbar, is exceptionally tight, as is typical of North Atlantic Central Water. Thermohaline intrusions are thus not likely to be a major stirring/mixing agent at the tracer injection level.

An HRP cruise in April of 1992 served as an initial site survey for the NATRE tracer injection. The HRP is a free-falling, internally recording vertical profiler (Schmitt et al. 1988). Relative velocities are measured with an acoustic velocimeter. Profiles of oceanic velocity are computed from relative velocity, accelerometer, and magnetometer data using a variation of the Total Ocean Profiling System (TOPS) model (Hayes et al. 1984). Temperature, conductivity, and pressure are sensed with an NBIS Mark III CTD. The HRP also carries a microstructure suite consisting of two airfoil shear probes and fast-response temperature and conductivity sensors. The NATRE HRP data are discussed in Polzin et al. (1995), Polzin (1996), St. Laurent and Schmitt (1999), and in a companion paper (Polzin et al. 2003). The latter paper discusses a decomposition of the finescale data into internal waves and subinertial motions that is explicitly utilized here. There is no evidence for submesoscale coherent vortices (meddies) at the level of the Mediterranean salt tongue (1000 m) in this initial site survey. We therefore feel justified in excluding their possible effect at the injection level.

Polzin et al. (2003) used a model for the interaction

of waves with quasi-permanent density finestructure (vortical modes) to decompose the observed vertical wavenumber (m) spectrum of vertical shear $S_z(m)$ and strain $F_z(m)$[1] into internal wave and vortical components. The vortical mode contribution to the vertical wavenumber strain spectrum was well captured by the parametric representation,

$$F_{z0} = \frac{A}{(1 + m_1^2/m^2)(1 + m^2/m_2^2)}. \quad (1)$$

The model parameters are $A = 3.14$ (cpm)$^{-1}$, $m_1 = 0.0550$ cpm, and $m_2 = 0.155$ cpm.

Following Polzin et al. (2003), the vortical mode shear spectrum can be estimated under the assumption that motions are balanced. This assumption neglects cyclostrophic effects (Kunze et al. 1990; Riley and Lelong 2000), which, if important, could lead to uncertainty in the estimate of the horizontal spectrum. Under quasigeostrophic scaling, shear is simply linked to strain via the thermal wind relation,

$$S_{z0} = B_r^2 \overline{N^2} F_{z0}, \quad (2)$$

where $B_r^2 \equiv \overline{N^2} k_h^2/f^2m^2$ is the Burger number squared, m and $k_h = (k^2 + l^2)^{1/2}$ are vertical and horizontal wavenumbers, (k, l) is the horizontal wave vector, and f and N are Coriolis and buoyancy frequencies. The average buoyancy and Coriolis frequencies for these data are $[\overline{N^2}]^{1/2} = 4.25 \times 10^{-3}$ s^{-1} and $f = 6.4 \times 10^{-5}$ s^{-1}.

The vortical mode analysis of Polzin et al. (2003) seems to support quasigeostrophic scaling, that is, a Burger number of order 1, and a small Rossby number. We thus use geostrophy to relate the vertical and horizontal spectra of vortical modes. Taking the ratio between shear and strain of vortical modes, one finds a characteristic aspect ratio of $B_r^2 = 1.6$. This relationship is used to relate vertical and horizontal wavenumbers, that is, $k_h = mfB_r/\sqrt{\overline{N^2}}$. We now convert (1) and (2) to horizontal wavenumber spectra via the relationship $E_k(k_h)dk_h = E_k(m)dm$ in which E_k represents the kinetic energy spectrum,

$$E_k(k_h) = \frac{\sqrt{\overline{N^2}}\, fB_r^3 E_0 k_h^{-2}}{(1 + k_{h1}^2/k_h^2)(1 + k_h^2/k_{h2}^2)} \quad (\text{m}^2\ \text{s}^{-2}/\text{rad m}^{-1}) \quad (3)$$

with $(k_{h1}, k_{h2}) = fB_r(m_1, m_2)/\sqrt{\overline{N^2}}$ and $E_0 = 0.25$ (rad/m)$^{-1}$.

There are no available estimates to quantitatively assess the assumption of a constant Burger number nor the assumption behind the quasi-permanent density finestructure model. The random error associated with the spectral estimates used to fit the parametric function in (1) is small (with 95% confidence levels of roughly ±50%). However, the bias errors associated with uncertainty in the model assumptions from which the spectrum is inferred are not known.

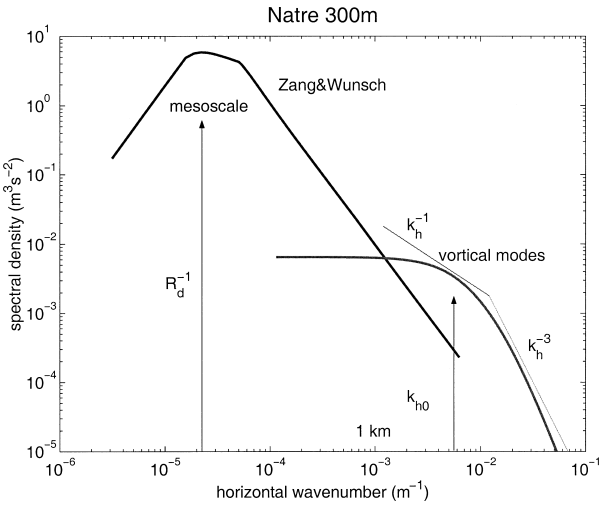

FIG. 2. Horizontal wavenumber velocity spectra $[2E_k(k_h)]$ from the vortical mode model (3) and the Zang and Wunsch (2001) model. The latter spectrum has been converted to its one-dimensional form. R_d is the mode-1 deformation radius (45 km) and k_{h0}^{-1} is the dominant horizontal scale defined from the energy content spectrum (Fig. 3). The thin lines above the vortical spectrum define power laws $k_h^{-\alpha}$ with $\alpha = 1$ and $\alpha = 3$. The local regime is defined by the energy density spectrum being tangent to $k_h^{-\alpha}$ with $1 < \alpha < 3$.

The resulting spectrum of horizontal velocity (shown in Fig. 2) is white, $E(k_h) \propto k_h^0$, at low wavenumber ($\lambda_h > 3$ km, $k_h < 2 \times 10^{-3}$ m^{-1}). The rms velocity $(u^2 + v^2)^{1/2}$ is small (0.007 m s^{-1}), relative to both the total subinertial mesoscale contribution (0.022 m s^{-1}) and to the superinertial internal wave contribution (0.048 m s^{-1}).

The horizontal spectrum intersects the steeper mesoscale spectrum of Zang and Wunsch (2001) at about $k_h = 1 \times 10^{-3}$ m^{-1}.[2] Vortical modes dominate the mesoscale tail and overwhelm the velocity gradients of the mesoscale eddy field. At the smallest scales, relative separation of particle pairs and tracer dispersion are a result of coherent straining by all turbulent motions. Given that vortical modes dominate the horizontal velocity gradients, vortical modes likely dominate the relative dispersion process at small scales. At scales larger

[1] Shear $[S_z(m)]$ is the vertical derivative of horizontal velocity (u_z, v_z). Strain $[F_z(m)]$ represents variability in buoyancy frequency squared normalized by the time mean $\overline{N^2}$, $[(N^2 - \overline{N^2})/\overline{N^2}]$, rather than any component of the rate of strain tensor of the isopycnal velocity field.

[2] Neither the Zang and Wunsch nor the vortical mode horizontal spectrum of horizontal velocity are actually measured. The Zang and Wunsch spectrum is a product of power law fits of an anisotropic spectrum to sea surface height and sea surface temperature data and the invocation of geostrophy to obtain horizontal velocity. Conversion of their 2D spectrum having $E_k(k, l) \propto (k^2 + l^2)(kl)^{-4}$ at high wavenumber to a one-dimensional spectrum returns $E_k(k_h) \propto k_h^{-2}$. The Zang and Wunsch spectral level is spatially variable. Here the spectral level has been set, so as to match the total subinertial kinetic energy measured in NATRE. The vortical mode velocity spectrum represents a simple conversion from the vertical displacement spectrum using a constant Burger number.

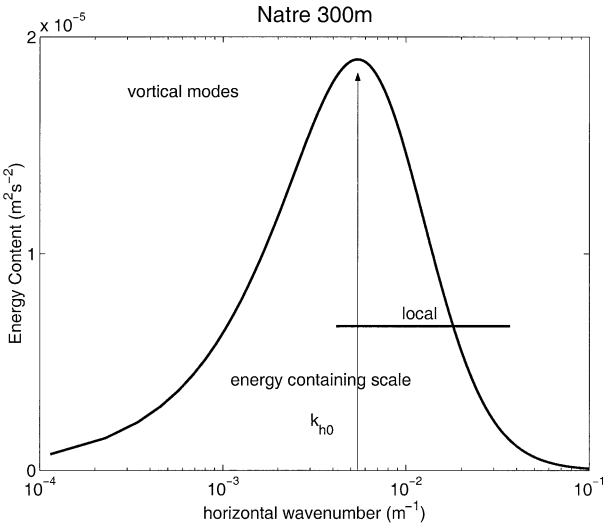

FIG. 3. Horizontal wavenumber velocity spectra $[2k_hE_k(k_h)]$ from the vortical mode model in a variance-preserving format. In this format the variance is proportional to the area under the curve. The peak in the energy content spectrum defines a scale k_{h0}^{-1}, which contributes most of the total variance.

than the spectral intersection, particle pairs still undergo an efficient straining process in response to mesoscale velocity gradients, whereas the response to gradients in the vortical field is an inefficient erratic sequence of small random steps much like a random walk.

Note that the intersection between vortical modes and mesoscale spectra shifts to a lower wavenumber if one were to chose a steeper spectrum $E(k_h) \propto k_h^{-3}$, as suggested by numerical studies of quasigeostrophic turbulence in the direct enstrophy cascade regime (Salmon 1998). However the shift of the intersection is small (a factor of 2 smaller), and there is not much observational evidence to support $E(k_h) \propto k_h^{-3}$. We will come back to this issue in the discussion section.

The vortical mode spectrum has a dominant horizontal scale ($\ell_0 = k_{h0}^{-1}$) of about 200 m (Fig. 3). This corresponds to horizontal and vertical wavelengths of 1.2 km and 25 m, respectively. One can anticipate from Fig. 3 that vortical modes act as an effective diffusivity at scales larger than the dominant scale (1 km). Vortical modes at large scales have little energy, and they act as small-scale random motions much like molecular agitation. It is well known that molecular agitation can be described as a random walk and represents a diffusive process with constant diffusivity. As the low-wavenumber energy is not important to the details of the dispersion process, the exact position of the intersection will not qualitatively affect the results discussed in this paper.

3. Isopycnal dispersion

In the previous section we described a partitioning of the along-isopycnal motions into ''fast'' internal waves and ''slow'' vorticity modes. Here we interpret the dispersive properties of vortical modes in the context of 2D turbulence. Our focus is to estimate the evolution of an ellipsoid marked with some tracer. This is done by estimating the spreading of particle pairs seeded in the tracer patch, through the 2×2 inertia tensor of $p(\mathbf{r}, t)$,

$$A_{p,ij}(t) = \int r_i r_j p(\mathbf{r}, t)\, d\mathbf{r}, \tag{4}$$

where $p(\mathbf{r}, t)$ is the probability density function for the spatial separation $\mathbf{r}$ of particle pairs and (r_1, r_2) are the two along-isopycnal coordinates.

It is not possible to formally derive a closed prognostic equation for $p(\mathbf{r}, t)$ and some approximations must be made. Excellent reviews of the various approaches proposed over the last 50 years can be found in Larcheveque and Lesieur (1981) and Bennett (1987). Here it suffices to say that, for a statistically stationary homogeneous and isotropic turbulent velocity field, it is possible to write an equation of the form,

$$\frac{\partial P(r, t - t_0; r_0)}{\partial t} = \frac{1}{r}\frac{\partial}{\partial r}\left[rD(r, t - t_0)\frac{\partial P(r, t - t_0; r_0)}{\partial r}\right], \tag{5}$$

for the radial dispersion of an initially isotropic distribution of particles in which $P(r, t - t_0; r_0)$ represents the probability that a pair of particles separated by r_0 at time t_0 have a separation of r at the later time t; D is the two-particle diffusivity, defined as the rate at which two particles separate along the line that separates them.[3] The approximations that enter in the derivation of (5) amount to either neglecting or parameterizing the triple correlations between particle displacements and velocities.

The details for the expression of the two-particle diffusivity D depend on the closure scheme. All closures, however, predict that D has the general form,

$$D(r, t - t_0) = \int_0^\infty dk_h\, E_k(k_h)\left[1 - \frac{2}{rk_h}J_1(rk_h)\right]\int_0^{t-t_0} R(k_h, \tau)\, d\tau \tag{6}$$

in which $E_k(k_h)$ is the isotropic 2D spectrum of the

[3] The full two-particle diffusivity $\mathcal{D}$ is a 2×2 tensor. For homogeneous and isotropic turbulent flows, the full tensor can be expressed in terms of the two-particle diffusivity along the particle separation $\mathbf{r}$, D, and the two-particle diffusivity perpendicular to the particle separation, $D_\dagger$. One can prove that the sum of the diagonal terms (the trace) of $\mathcal{D}$ is given by, $\mathrm{Tr}\{D\} = 2D + r\, dD_\dagger/dr$. We refer to D as two-particle diffusivity, but often this name is used for $\mathrm{Tr}\{D\}$. We will point out where confusion between the two definitions might arise.

velocity field and J_1 is the Bessel function of order 1; $R(k_h, \tau)$ is the Lagrangian correlation time for eddies of wavenumber k_h. Because of homogeneity, isotropy, and stationarity, D depends only on the absolute particle separation $r = |\mathbf{r}|$ and on the time $t - t_0$ since release.

The expression in (6) can be interpreted as a two-particle extension of Taylor's formula for the single-particle diffusivity. Single-particle diffusivity describes the meandering of a single particle in a turbulent flow. Two-particle diffusivity describes the separation of particle pairs and is related to the growth in size of a tracer patch. Taylor's formula states that the one-particle diffusivity is given by the product of the eddy kinetic energy and the Lagrangian correlation function integrated from time zero up to time t. The two-particle expression is also the product of the eddy kinetic energy $E_k(k_h)$ and the time integral of the Lagrangian correlation function for eddies of wavenumber k_h. However, in (6) there is a weighting factor $1 - 2(rk_h)^{-1} J_1(k_h r)$ in the integral over the wavenumbers k_h. This factor is close to unity for $k_h r \gg 1$ and acts as a differential operator for $k_h r \ll 1$ because $[1 - 2(rk_h)^{-1} J_1(k_h r)] \approx k_h^2 r^2/8$. Physically, this weighting states that eddies of wavenumber $k_h r \ll 1$ tend to separate particles by coherent straining (two-particle dispersion), while eddies with $k_h r \gg 1$ result in the two particles executing independent random walks (one-particle dispersion).

Suppose now that two particles are released at $t = t_0$ so close to each other that their separation r lies in the high-wavenumber subrange of the vortical mode spectrum in (3). That is, r is smaller than the energy-containing scale introduced in Fig. 3 and $rk_{h0} < 1$. In this subrange, the dynamics appear to be local in wavenumber space because the vortical mode spectrum is tangent to $k_h^{-\alpha}$ with $1 < \alpha < 3$ (Bennett 1984). Given local dynamics and sufficiently long t, the integral over τ in (6) becomes an integral time scale, which may be estimated using self-similar arguments:

$$\int_0^\infty R(k_h, \tau)\, d\tau \sim E_k(k_h)^{-1/2} k_h^{-3/2}. \tag{7}$$

For $\alpha > 3$, the approximation in (7) is not valid as the integral is dominated by scales larger than k_h. For $\alpha < 1$, the integral does not converge and dispersion is controlled by the dominant length scale of the energy spectrum. That is, two-particle dispersion has attained its absolute limit. It is not clear that (7) holds long before the particle separation is as big as the energy-containing eddies, but Bennett (1984) reports that it is well supported by numerical experiments in two-dimensional turbulence. We assume the $O(1)$ constant relating the left and right-hand sides of (7) to be unity.

Once the two particles drift farther apart than the energy-containing scale, $r \sim k_{h0}^{-1}$, the vortical mode spectrum flattens ($\alpha < 1$) and the dynamics become nonlocal. In this range the integral over k_h in (6) is dominated by energy at wavenumber k_{h0} and dispersion is absolute rather than relative. The two-particle diffusivity asymptotes to a constant, $D = \frac{1}{2}U^2 \tau_L$, where $\frac{1}{2}U^2$ is the total kinetic energy and τ_L the Lagrangian integral time scale. This is the long-time limit of Taylor's formula.[4] If the integral time scale is estimated as the ratio of the dominant length scale and the rms velocity, $\tau_L = \ell/(u^2 + v^2)^{1/2}$, then $D = 0.007\ \text{m s}^{-1} \times 200\ \text{m} = 1.4\ \text{m}^2\ \text{s}^{-1}$.

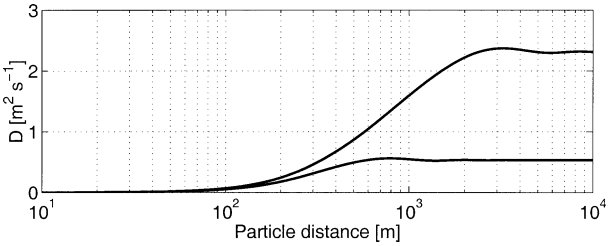

FIG. 4. Two-particle diffusivity D in a vortical mode field as given by (6). The values of D saturate for large r because we consider only the contribution due to vortical modes; i.e., we truncate the spectra of the advecting velocity field below the wavenumber $k_{h\text{cut}}$. In the real ocean the two-particle diffusivity keeps growing with scale because of the straining by mesoscale eddies at wavenumbers below $k_{h\text{cut}}$. The scale at which the curves of D saturate determines the separation r beyond which the effect of vortical modes can be represented as an effective constant diffusivity. The two different lines correspond to different choices of $k_{h\text{cut}}$: the upper line is obtained by setting $k_{h\text{cut}}$ equal to the scale at which the vortical mode spectrum intersects the mesoscale spectrum as estimated by Zhang and Wunsch (Fig. 2). The lower line is obtained by setting $k_{h\text{cut}} = k_{h0}$, i.e., the energy-containing scale of vortical modes.

Given the nonlocal nature of the vortical spectrum (3) at low wavenumber, (6) is not valid unless the lower limit of integration is moved away from $k_h = 0$ to a critical wavenumber $k_{h\text{cut}}$. The definition of this wavenumber is imprecise. With reference to Figs. 2 and 3, plausible choices for $k_{h\text{cut}}$ can range from 1) the energy-containing scale of vortical modes k_{h0} to 2) the intersection between the vortical modes and the eddy field spectra. In both cases, the two-particle diffusivity associated with vortical modes is estimated by setting $E_k(k_h)$ to zero for $k_h \leq k_{h\text{cut}}$ in (6).

In Fig. 4, we sketch D (6) for both choices of the lower cutoff. The effect of vortical modes is to induce a rapid growth of the two-particle diffusivity on scales between 100 m and 1–2 km. On larger scales the eddy diffusivity asymptotically approaches a value between 0.5 and 2.5 $\text{m}^2\ \text{s}^{-1}$ depending on the choice made for $k_{h\text{cut}}$. Note that the two-particle diffusivity in the real ocean keeps growing at scales larger than a few kilometers because of strain in the mesoscale field. However, in our calculation we are considering only the effect of vortical modes. The scale at which the two-particle diffusivity plotted in Fig. 4 saturates indicates

[4] Here D is the along-separation, two-particle diffusivity and asymptotically approaches the one-particle diffusivity. The trace of the full two-particle diffusivity asymptotically approaches 2 times the one-particle diffusivity.

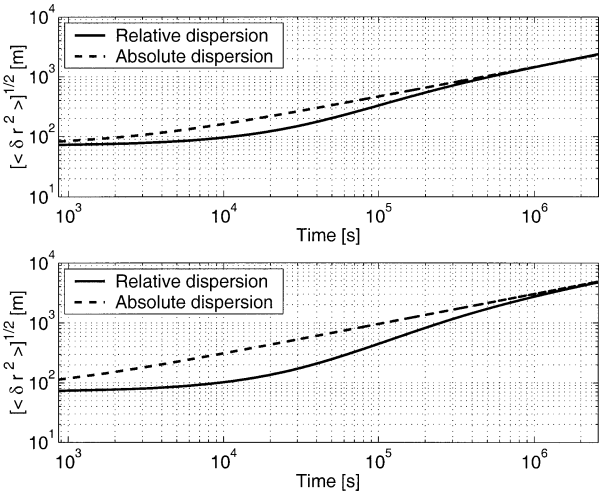

FIG. 5. Growth rate of the rms displacement of particle pairs deposited in a cloud of tracer (solid line). The displacement is estimated as radius $A_p(t)$ from (6). The upper panel corresponds to the lower estimate of diffusivity in Fig. 4 and the lower panel to the higher estimate. The dashed line depicts the long-term growth of the cloud in the absolute dispersion limit, $D = D(r = \infty, t - t_0 = \infty)$.

the scale at which dispersion due to vortical modes can be described by a constant eddy diffusivity. The main result is that stirring associated with vortical modes on scales between a few hundred meters and a few kilometers is on the order of 1 $m^2\ s^{-1}$ and not 0.01 $m^2\ s^{-1}$ as one would expect if the only process acting on those scales was internal wave-induced dispersion (Young et al. 1982; Ledwell et al. 1998; Ferrari 2003, unpublished manuscript).

Now that we have an estimate for the two-particle eddy diffusivity, we can attempt to evaluate the growth rate of a tracer patch released in a vortical mode field. Let us consider a tracer patch whose concentration is a Gaussian circular blob with a standard deviation $\sigma =$ 25 m. We seed this patch with particles distributed as a Gaussian with the same standard deviation; the corresponding distribution of particle displacements $p(r_0)$ is a Gaussian with $\sigma = \sqrt{2} \times 25$ m. Thus we set $P(r, t = 0; r_0) = p(r_0)$ and solve equation (5). By computing the integral in (4) at different times, we can track the growth of the area occupied by particles. In Fig. 5 we plot the radius of A_p as a function of time. The two panels show respectively the results obtained with the lower and upper values of the diffusivity in Fig. 4. The growth rate of A_p is extremely fast during the initial transient, but after 5–10 days it starts growing linearly in time as the two-particle statistics asymptote to the single-particle statistics.

The patch size to be inferred from Fig. 5 should not be read as a detailed description for any particular tracer release experiment during the first few days. The important information is that the tracer patch continues its explosive growth for 5–10 days. During this initial transient, the tracer patch is formed by a few individual streaks emanating from the release spot. Only as the two-particle and absolute dispersion estimates converge (a couple of weeks; Fig. 5) do the streaks wrap around and form a web of contorted filaments that collectively spread as the square root of time. In this stage ensemble averages are meaningful to describe the patch as a whole, but not the details of individual streaks. The ensemble estimates give a blurred picture of the patch; only the mean-square variance is predicted.

We can now compare the effect of vortical modes with that of mesoscale eddies. The Zang and Wunsch (2001) spectrum has a k_h^{-2} dependence at high wavenumber. If one is to believe this form for the spectrum, the local regime used in this section to estimate D applies also for the mesoscale field. Since locality implies that dispersion at each scale is dominated by the energy density of the velocity field at that scale, simple inspection of Fig. 2 implies dispersion by vortical modes dominates dispersion associated with the Zang and Wunsch (2001) spectrum at scales smaller than 1 km. However this result depends upon whether one accepts the high-wavenumber fits of Zang and Wunsch. Those authors note that their high-wavenumber fits should be viewed with caution. Note, as well, that their spectrum is anisotropic at all scales, whereas one might expect nonlinearity to lead to small-scale isotropy. We will return to these issues in the discussion of our results.

The present analysis is clearly subject to a number of assumptions dictated by the limited information available on vortical modes. Nonetheless we believe that two main results are robust: vortical modes induce an eddy diffusivity of $O(1)$ $m^2\ s^{-1}$ on scales of $O(1)$ km and a tracer patch gets distorted into an intricate web of filaments within a two-week time.

4. The tracer release experiment

Because interpretation of the tracer release is an integral part of this study, we summarize Ledwell et al.'s (1998) results in sufficient detail to motivate our analysis. The reader is directed to that paper for further description, interpretation of the tracer data, and insight into its limitations.

The tracer was injected (Fig. 6) as a set of nine streaks from a towed vehicle over the time period of 5–13 May 1992 and sampled immediately thereafter over the period of 14–31 May, an average time difference of two weeks (1.2×10^6 s). Subsequent sampling took place in October and November of 1992, April and May of 1993, and November of 1994. Our interest is confined to the injection and first two surveys.

The injection determines the initial conditions for our estimates of subsequent dispersion. The estimated rms spread about the injection isopycnal associated with the injection process was smaller than 2 m. The estimated lateral dispersion of the tracer associated with the turbulent wake of the injection apparatus was 25 m, but might be as large as 100 m or as small as 10 m (J.

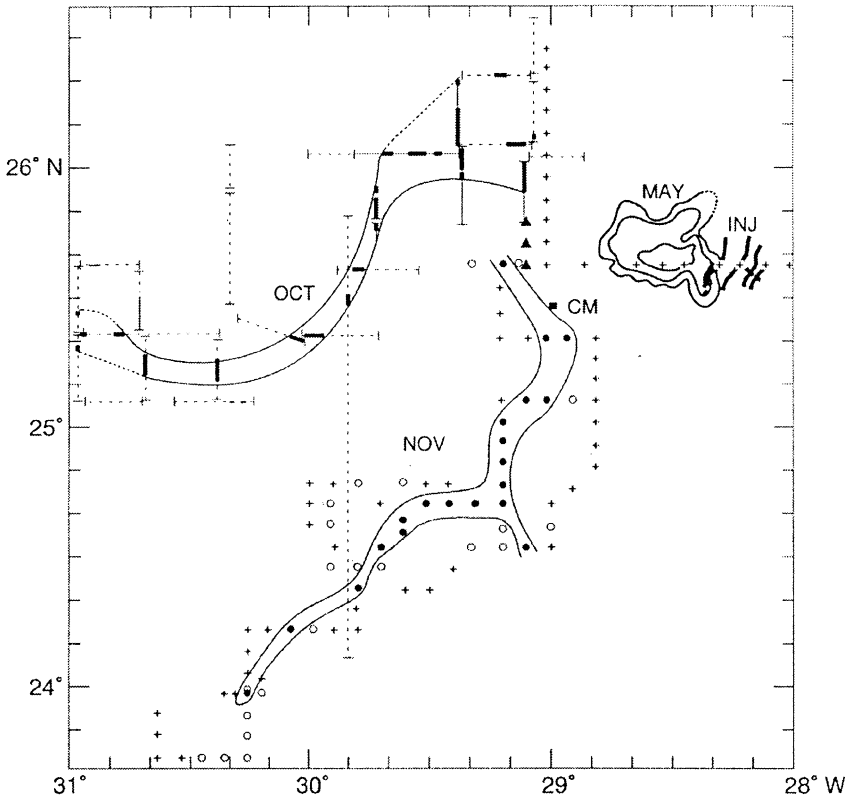

FIG. 6. Column-integrated tracer concentrations from NATRE. Injection streaks are shown as short heavy lines near 26°N, 28°W. Closed contours just to the west define a smoothed map of the patch at the initial (2 week) survey. The sinuous features to the west and southwest define tracer filaments encountered during the six-month survey. Point CM marks the location of the subduction experiment central mooring. (Figure courtesy of Jim Ledwell, with permission from *Nature,* Vol. 364, p. 701, Copyright 1993 MacMillan Magazines Ltd.)

Ledwell 2002, personal communication). The estimates presented in Fig. 5 use an initial condition of $r_0 = 25$ m. The nine streaks had an initial overall length (L_i) of about 100 km and an initial separation of about 5 km (Fig. 6). These nine streaks defined an initial patch of about 25×25 km^2 extent.

The horizontal dispersion of the tracer at the two-week interval was assessed with a multichamber sampling system towed along the injection isopycnal (Fig. 7), with each sample returning an average concentration estimate over 200–600 m of the tow track. At two weeks, the tracer streaks had formed a nearly continuous patch (Fig. 6) that had been stretched zonally and compressed meridionally by a factor of 2 or so. The tracer distribution was not smooth, however (Fig. 7). Ledwell et al. interpret features within the patch as, ''streaks that had been stretched, reoriented, and distorted at scales greater than a few kilometers and that had been broadened in the cross-streak direction at smaller scales.'' Over 40 crossings of the original streaks were identified from 42 tows of the sampling system, and from these crossings an rms cross-streak width of $W_{14\text{ days}} = 300 \pm 100$ m was obtained. Note that the analysis of the streaks is subjective, the data are gappy, and the resulting estimates of streak width are at the nominal resolution of the sampling apparatus. However, Ledwell et al. state that the streak widths appear to grow in time over the initial sampling period. This would not be the case if the streak widths were underresolved. After this two weeks, the total streak length was estimated as $L_{14\text{ days}} = 250$ km. Last, it was difficult to map the observed streak crossings into a structure that could be identified as resulting from the initial nine streaks (J. Ledwell 2002, personal communication). That is, the observed streaks at the two-week sampling interval were so convoluted that the initial condition cannot be reconstructed.

By October–November of 1992 the mesoscale eddy field had teased the tracer patch into elongated filaments (Fig. 6). There was a clear distinction between the tracer containing filaments and surrounding water. Sampling of the tracer in October of 1992 again utilized a towed vehicle. The sampling was somewhat modified so that average concentrations over 600 m at the injection isopycnal were obtained. Sampling during November was done with conventional rosette casts and Niskin bottles at a 9-km station spacing. Ledwell et al. infer the total filament length to be $L_{6\text{ months}} = 1800$ km and, from the

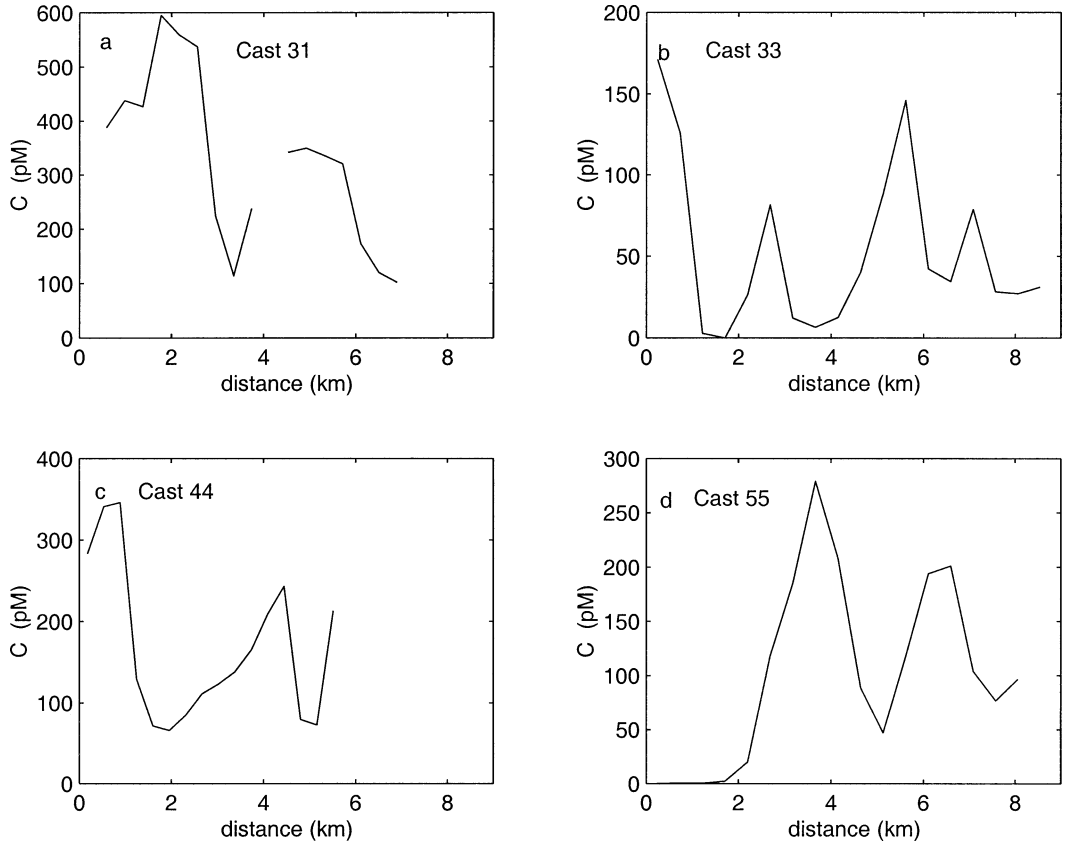

FIG. 7. Tracer concentrations from the multichamber sampling system at the injection isopycnal. (Data from J. Ledwell 2002, personal communication.)

October tows, an rms streak width of $W_{6\text{ months}} = 3$ (2–5) km. Little structure was observed within or at the edges of the filaments at this point. This may have been a result of the increased sampling interval or typically lower concentration levels in combination with greater contamination of the samples (J. Ledwell 2002, personal communication).

The basis for Ledwell's estimate of isopycnal diffusivity was to consider the evolution of a tracer with concentration c in a uniform strain field $(u, v) = (-\Gamma x, \Gamma y)$,

$$c_t - c_x\Gamma x + c_y\Gamma y = D\nabla^2 c. \tag{8}$$

In this representation, the x and y axis represent the straining and compressing directions of the rate of strain. The rms length and width of a filament are given by the equations for the normalized second moments of c:

$$\partial_t\langle x^2c\rangle + 2\Gamma\langle x^2c\rangle = 2D \quad \text{and} \tag{9}$$

$$\partial_t\langle y^2c\rangle - 2\Gamma\langle y^2c\rangle = 2D. \tag{10}$$

After an initial transient, the length $\langle y^2c\rangle$ of a filament grows exponentially as $\exp(2\Gamma t)$, while the width reaches a balance between strain and diffusion $\langle x^2c\rangle \approx D/\Gamma$.

Following (Garrett 1983), Ledwell et al. (1998) use their estimates of streak length to produce an estimate of the rate of strain:

$$\begin{aligned}\Gamma_{14\text{ days}} &= \log(L_{14\text{ days}}/L_i)/14\text{ days}\\ &= (8 \pm 4) \times 10^{-7}\text{ s}^{-1} \quad \text{and}\\ \Gamma_{6\text{ months}} &= \log(L_{6\text{ months}}/L_i)/6\text{ months}\\ &= (3 \pm 0.5) \times 10^{-7}\text{ s}^{-1}.\end{aligned}$$

Ledwell et al. note that the resulting rate of strain estimate ($\Gamma_{14\text{ days}}$) is not expected to be uniform in time or space, and go so far as to suggest a contribution to $\Gamma_{14\text{ days}}$ associated with motions *within* the patch.

The cross-streak widths were then assumed to represent a balance between straining and diffusion:

$$\begin{aligned}D_{14\text{ days}} &= \Gamma_{14\text{ days}} \times W^2_{14\text{ days}}\\ &= 0.07 \pm 0.04\text{ m}^2\text{ s}^{-1} \quad \text{and}\\ D_{6\text{ months}} &= \Gamma_{6\text{ months}} \times W^2_{6\text{ months}}\\ &= 3(1 - 10)\text{ m}^2\text{ s}^{-1}.\end{aligned}$$

Sundermeyer and Price (1998) argue that the rate of strain Γ in (9) and (10) is given by $\Gamma = \Gamma_{6\text{ months}}/2$ so that $\Gamma\langle x^2c\rangle = 2(0.6–6)\text{ m}^2\text{ s}^{-1}$ (Ledwell et al. 1998).

This quantitatively agrees with our asymptotic estimates of the rate of vortical mode dispersion,

$$D(t - t_0 = \infty) = 0.5\text{–}2.5 \text{ m}^2 \text{ s}^{-1}.$$

Conversely, use of our dispersion estimates in (9) returns a prediction for the rms streak width (2–4 km), which agrees with the 6-month observations.

5. Discussion

a. Interpretation

Our interpretation of these tracer observations is as follows. The use of (9) and (10) assumes that, first, the stirring process represented by Γ and the turbulent diffusion process represented by D operate on two different scales and, second, the tracer patch has a size intermediate between those two scales. At the two-week sampling interval, use of this model to interpret the vortical mode results (Figs. 4 and 5) is misleading because there is no scale separation between the size of the tracer patch and the vortical turbulent motions: the streak widths ($W_{14 \text{ days}} = 300 \pm 100$ m) are nearly the same as the vortical mode dominant scale $k_{h0}^{-1} = 200$ m. That the two-week diffusivity has already reached its asymptotic value of $D(t - t_0 = \infty) = 0.5 - 2.5 \text{ m}^2 \text{ s}^{-1}$ and far exceeds the tracer-inferred value of $D_{14 \text{ days}} = 0.07 \pm 0.04 \text{ m}^2 \text{ s}^{-1}$ is inconsequential. The $D(t - t_0 = \infty) = 0.5\text{–}2.5 \text{ m}^2 \text{ s}^{-1}$ values describe the evolution of the envelope of filaments, while the tracer-inferred values $D_{14 \text{ days}}$ are an attempt to interpret the individual filament widths.

We believe the convoluted structure of the observed tracer field represents the web of intertwined filaments associated with vortical mode stirring described in section 3. The mesoscale rate of strain is responsible for distorting and reorienting the initial 25×25 km^2 patch by a factor of 2 or so. However, the mesoscale has insufficient structure and decorrelation time scales that are too large to create the variability on the scales apparent in Fig. 7 (see below). In contrast, the two weeks between injection and sampling is sufficient for the vortical mode two-particle statistics to approach their single-particle counterparts. This implies sufficient time for the filaments to wrap around themselves and create a convoluted web. Our estimates of the rms separation [$(\sqrt{A_p}(t = 14 \text{ days}) = 2\text{–}4$ km] are sufficiently large as to imply a merging of the nine initial tracer filaments.

Curiously, we find the streaks to be separated by a distance slightly larger than what we infer as 2π times the vortical mode dominant scale. Numerical simulations (Holloway and Kristmannsson 1984) suggest a tendency for tracer fluxes to be dominated by contributions at scales slightly larger than the dominant eddy scale and many depictions of passive tracer distributions in the literature appear to compare favorably with our interpretation of a finescale tracer web.

b. Mesoscale eddies

At the two-week sampling interval the patch was obviously deformed by a factor of 2 or so, presumably by the mesoscale. Our kinematic split in the spectral domain between vortical modes and the mesoscale eddy field ignored this interaction. This kinematic split is justified if the mesoscale spectrum has a k_h^{-2} slope, as suggested by Zhang and Wunsch (2001). In this scenario dispersion is local; that is, it is dominated at each scale by the kinetic energy density at that scale, both in the mesoscale and in the vortical mode regimes. Thus at subkilometer scales dispersion is dominated by the more energetic vortical mode component, while at larger scales the mesoscale eddy field dominates.

On closer inspection, though, the tracer observations cast some doubts on the spectral slope proposed by Zhang and Wunsch. Filamentation is evident after 6 months for scales above a few kilometers, while the tracer is well homogenized on smaller scales. A nonlocal stirring field creates strong filamentation down to scales where other processes remove variance. This limit is well studied in the literature on chaotic advection (Ottino 1988). The opposite happens in the local limit: the velocity field decorrelates so fast that filaments do not survive for long and tend to wrap up and homogenize the tracer (Falkovich et al. 2001). The picture that emerges at 6 months after release is consistent with a nonlocal mesoscale spectrum that creates filaments down to scales of a few kilometers and a local vortical mode spectrum that homogenizes the tracer on smaller scales. In order for this picture to work, the vortical modes must be strong enough to arrest the filamentation due to mesoscale motions.

The relative dispersive strength of vortical modes and mesoscale eddies, in the limit of steep mesoscale spectra, can be estimated as follows. Classical theory of two-dimensional and quasigeostrophic turbulence in the direct enstrophy cascade predicts spectral slopes of k_h^{-3} (Kraichnan 1966). A straightforward implication is that the two-particle diffusivity scales like

$$D(r) \propto \eta^{1/3} r^2, \tag{11}$$

where η is a constant entrophy flux. Observations suggest that $D(100 \text{ km}) \approx 1000 \text{ m}^2 \text{ s}^{-1}$. According to the scaling in (11) then $D(1 \text{ km}) \approx 0.1 \text{ m}^2 \text{ s}^{-1}$, which is an order of magnitude smaller than the two-particle diffusivity due to vortical modes. Thus, vortical modes dominate dispersion at small scales, even if one accounts for nonlocal effects caused by mesoscale eddy field.

c. Generation and evolution of the vortical field

The vortical spectrum is interpreted here as a product of both nonlinear interactions and forcing. Polzin et al. (2003) suggest that vortical modes in this dataset represent buoyancy anomalies resulting from internal wavebreaking. Turbulent patches of over 20-m vertical

extent are apparent in the microstructure data (e.g., Polzin 1996). Given a rough equivalence between internal wave and patch aspect ratios (Marmarino et al. 1985; Osborn and Lueck 1985) and an inferred internal wave aspect ratio of $0.5f/\sqrt{\overline{N^2}}$ (Polzin et al. 2003), internal wavebreaking could easily force buoyancy anomalies with horizontal scales of 1 km. As a combination of both forcing and nonlinearity, the spectral slopes of the vortical mode spectrum need not correspond to the classical inverse energy [$E(k_h) \propto k_h^{-5/3}$] or enstrophy cascade [$E(k_h) \propto k_h^{-3}$] subranges.

d. Geographic variability

The result we have obtained may be rather peculiar to the southeastern portion of the North Atlantic subtropical gyre. If vortical motions are substantially forced by internal wave breaking, the geographic variability in the open ocean thermocline removed from bathymetry may be small. The same cannot be said of the mesoscale eddy field. If the mesoscale spectrum was a factor of 100 larger, as is the case in the more energetic portions of the subtropical gyre (Zang and Wunsch 2001), dispersion by eddies on the submesoscale may well overwhelm any signature of dispersion by vortical motions. As we learn more about vortical mode climatology, (9) can be used to define the arrest scale.

6. Summary

The release of an anthropogenic tracer on an isopycnal at about 300-m depth in the southeastern part of the North Atlantic subtropical gyre returned a unique picture of isopycnal dispersion. Ledwell et al. (1998) found the following.

- The initial tracer streaks, less than 100 m wide and 5 km apart, had blended into one nearly continuous patch within two weeks of the release. The tracer distribution was not smooth, however. The patch consisted of streaks having width of 300 $\pm$ 100 m and separation of several kilometers.
- The initial patch was teased into a set of sinuous streaks separated by tracer-free water within several months. The cross-streak dimension of 3 (2–5) km was interpreted as being set by a balance between the mesoscale rate of strain tending to compress the cross-streak dimension and a smaller scale isopycnal dispersion tending to increase the streak width. Ledwell et al. estimate a dispersion coefficient of $D_{6\,\text{months}} \cong 2\ \text{m}^2\ \text{s}^{-1}$(0.6–6.0 $\text{m}^2\ \text{s}^{-1}$).

The tracer release was preceded by a fine- and microstructure survey. A decomposition of the finescale velocity and density fluctuations into internal waves and vorticity-carrying perturbations, called vortical modes (Polzin et al. 2003), quantifies the nonpropagating vortical field that can support persistent relative motion in a Lagrangian framework. Having only a spectral description of vortical modes, we used a second moment (spectral) scheme to estimate the dispersive properties of the vortical field. We found that

- an initial spot release of radius 25 m would be teased into filaments that fold back upon themselves to create a convoluted web of tracer with radius 2–4 km after two weeks and
- after 5–10 days stirring, in the vortical field can be described as a dispersion coefficient $D = 0.5$–$2.5\ \text{m}^2\ \text{s}^{-1}$.

We further note the following: 1) at two weeks, individual tracer streaks are separated by a length that is approximately 2π times the energy-containing scale in the vortical field and 2) there are many points of uncertainty in the analysis. The most problematic of these is the assumption of balanced vortical motions.

Vortical mode dispersion is not the only process that could be capable of producing enhanced diffusivities. Dispersion can arise as a second-order effect in a random internal wavefield (e.g., Sanderson and Okubo 1988; Weichman and Glazman 2000; Ferrari 2003, unpublished manuscript), but this process is very inefficient, achieving diffusivities of at most 0.01 $\text{m}^2\ \text{s}^{-1}$ for the background internal wave spectrum. Haynes and Anglade (1997) and Haynes (2001) suggest that vertical shear in the mesoscale eddy field coupled to vertical diffusion (shear dispersion) could be associated with $O(1\ \text{m}^2\ \text{s}^{-1})$ dispersion coefficients. Our primary misgiving of such a mechanism is that, acting in isolation of a small-scale stirring process, it would not be able to create the rich finestructure evident in the tracer distribution at two weeks.

Our assessment is that vortical modes can explain both the $O(1\ \text{m}^2\ \text{s}^{-1})$ dispersion coefficients estimated from the dispersion of an anthropogenic tracer during NATRE and the convoluted structure observed subsequent to its release. Mesoscale eddies cannot accomplish the later. Clearly, a combination of numerical simulations and more information on the spatial/temporal evolution of vortical modes is called for.

Acknowledgments. Chris Garrett forwarded an interesting argument for assessing the initial evolution of relative dispersion in a random strain field. This argument ultimately resulted in the isopycnal stirring analysis. Author K. Polzin gratefully acknowledges the support of NSF and ONR for the acquisition and analysis of these data; R. Ferrari was supported by the Postdoctoral Scholar Fellowship of WHOI.

REFERENCES

Bennett, A. F., 1984: Relative dispersion: Local and nonlocal dynamics. *J. Atmos. Sci.,* **41,** 1881–1886.

——, 1987: A Lagrangian analysis of turbulent diffusion. *Rev. Geophys.,* **25,** 799–822.

Falkovich, G., K. Gawedzki, and M. Vergassola, 2001: Particles and fields in fluid turbulence. *Rev. Mod. Phys.,* **73,** 913–975.

Garrett, C., 1983: On the initial streakiness of a dispersing tracer in two- and three-dimensional turbulence. *Dyn. Atmos. Oceans,* **7,** 265–277.

Hayes, S. P., H. B. Milburn, and E. F. Ford, 1984: TOPS: A free-fall velocity and CTD profiler. *J. Atmos. Oceanic Technol.,* **1,** 220–236.

Haynes, P. H., 2001: Vertical shear plus horizontal stretching as a route to mixing. *From Stirring to Mixing in a Stratified Ocean: Proc. 'Aha Huliko'a Hawaiian Winter Workshop,* Honolulu, HI, University of Hawaii at Manoa, 73–80.

——, and J. Anglade, 1997: The vertical-scale cascade of atmospheric tracers due to large-scale differential advection. *J. Atmos. Sci.,* **54,** 1121–1136.

Holloway, G., and S. S. Kristmannsson, 1984: Stirring and transport of tracer fields by geostrophic turbulence. *J. Fluid Mech.,* **141,** 27–50.

Kraichnan, R. H., 1966: Dispersion of particle pairs in homogeneous turbulence. *Phys. Fluids,* **9,** 1937–1943.

Kunze, E., A. J. Williams III, and M. G. Briscoe, 1990: Interpreting shear and strain finestructure from a neutrally buoyant float. *J. Geophys. Res.,* **95,** 18 111–18 126.

Larcheveque, M., and M. Lesieur, 1981: The application of eddy-damped Markovian closures to the problem of dispersion of particle pairs. *J. Mech.,* **20,** 113–134.

Ledwell, J. R., A. J. Watson, and C. S. Law, 1998: Mixing of a tracer in the pycnocline. *J. Geophys. Res.,* **103,** 21 499–21 529.

Marmarino, G. O., L. J. Rosenblum, J. P. Dugan, and C. Y. Shen, 1985: Temperature fine-structure patches near an upper ocean density front. *J. Geophys. Res.,* **90,** 11 799–11 810.

Osborn, T. R., and R. G. Lueck, 1985: Turbulence measurements from a towed body. *J. Atmos. Oceanic Technol.,* **2,** 517–527.

Ottino, J. M., 1988: *The Kinematics of Mixing: Stretching, Chaos, and Transport.* Cambridge University Press, 354 pp.

Polzin, K. L., 1996: Statistics of the Richardson number: Mixing models and finestructure. *J. Phys. Oceanogr.,* **26,** 1409–1425.

——, J. M. Toole, and R. W. Schmitt, 1995: Finescale parameterizations of turbulent dissipation. *J. Phys. Oceanogr.,* **25,** 306–328.

——, E. Kunze, J. M. Toole, and R. W. Schmitt, 2003: The partition of finescale energy into internal waves and subinertial motions. *J. Phys. Oceanogr.,* **33,** 234–248.

Provenzale, A., 1999: Transport by coherent barotropic vortices. *Annu. Rev. Fluid Mech.,* **31,** 55–93.

Rhines, P. B., 1979: Geostrophic turbulence. *Annu. Rev. Fluid Mech.,* **11,** 401–441.

Riley, J. J., and M.-P. Lelong, 2000: Fluid motions in the presence of strong stable stratification. *Annu. Rev. Fluid Mech.,* **32,** 613–658.

Salmon, R. L., 1998: *Lectures on Geophysical Fluid Dynamics.* Oxford University Press, 378 pp.

Sanderson, B. G., and A. Okubo, 1988: Diffusion by internal waves. *J. Geophys. Res.,* **93,** 3570–3582.

Schmitt, R. W., J. M. Toole, R. L. Koehler, E. C. Mellinger, and K. W. Doherty, 1988: The development of a fine- and microstructure profiler. *J. Atmos. Oceanic Technol.,* **5,** 484–500.

St. Laurent, L., and R. W. Schmitt, 1999: The contribution of salt fingers to vertical mixing in the North Atlantic Tracer Release Experiment. *J. Phys. Oceanogr.,* **29,** 1404–1424.

Sundermeyer, M. A., and J. F. Price, 1998: Lateral mixing and the North Atlantic Tracer Release Experiment: Observations and numerical experiments of Lagrangian particles and a passive tracer. *J. Geophys. Res.,* **103,** 21 481–21 497.

Weichman, P. B., and R. E. Glazman, 2000: Passive scalar transport by traveling wave fields. *J. Fluid Mech.,* **420,** 147–200.

Young, W. R., P. B. Rhines, and C. J. R. Garrett, 1982: Shear-flow dispersion, internal waves and horizontal mixing in the ocean. *J. Phys. Oceanogr.,* **12,** 515–527.

Zang, X., and C. Wunsch, 2001: Spectral description of low-frequency oceanic variability. *J. Phys. Oceanogr.,* **31,** 3073–3095.